PROCEEDINGS OF SCIENCE

Steps toward the 5FGL Fermi-LAT source catalog

Jean Ballet,[a,*] **Philippe Bruel,**[b] **Toby H. Burnett,**[c] **Jean-Marc Casandjian**[a] **and Matthew Kerr**[d] **on behalf of the Fermi-LAT collaboration**

[a] *Université Paris Saclay and Université Paris Cité, CEA, CNRS, AIM, F-91191 Gif-sur-Yvette, France*
[b] *Laboratoire Leprince-Ringuet, Ecole polytechnique, CNRS/IN2P3, F-91128 Palaiseau, France*
[c] *Department of Physics, University of Washington, Seattle, WA 98195-1560, USA*
[d] *Space Science Division, Naval Research Laboratory, Washington, DC 20375–5352, USA*

E-mail: Jean.Ballet@cea.fr

The current Fermi-LAT source catalog (4FGL-DR4: 7194 sources over 14 years) was built incrementally from the 8-year catalog. In a survey mission like Fermi, data accumulate on each source over time, so after 16 years (reached in August 2024) and twice the data for the original 4FGL sources we have much more precise localization. It is then time to generate a new original catalog (5FGL), which implies, beyond adding the sources newly detectable after two more years, changing the existing source names (derived from their coordinates) and reviewing the associations.

The systematic errors due to our imperfect knowledge of the Galactic diffuse emission, which dominates the gamma-ray sky, are the major limiting factor of the sensitivity and quality of the point source catalog at low energies (a few 100 MeV over the extragalactic sky, up to a few GeV in the Galactic ridge). Two parallel efforts are ongoing to improve on this situation, using more advanced methods to modulate the interstellar gas templates with the LAT data themselves.

In parallel an early 16-year list (FL16Y) of 7217 sources is presented, which relocalizes all sources and improves a few aspects of the catalog analysis, but still uses the same diffuse model as 4FGL-DR4.

39th International Cosmic Ray Conference (ICRC2025)
15–24 July 2025
Geneva, Switzerland

*Speaker

PoS(ICRC2025)560

1. Introduction

The current Fermi-LAT source catalog [4FGL-DR4: 1, 2] was built incrementally from the 8-year catalog [3]. This means that, except for a few specific cases, the positions of the original (DR1) sources (and their error ellipses) were frozen to what they were after eight years. Among the 7194 DR4 sources, about 300 were inherited from former 4FGL catalogs but formally below the detection threshold, and nearly 600 had moved outside their 95% error radius when considering the new seed localization, way beyond 5%. So we considered that the concept of incremental catalog reached its limit, and we had to build a fresh one.

The major limitation of the current LAT catalogs is the precision of the diffuse model. It is estimated at 3%, which is good but not enough for the statistical precision reached below 1 GeV, particularly in the Galactic Ridge. Therefore a full 5FGL will wait until we can provide a new diffuse model. Progress toward that goal is described in Section 2. In the meantime we provide an interim source list, that we call FL16Y (for Fermi-LAT 16-year), using the previous diffuse model. Preliminary results are described in Section 3.

2. Improvements to the interstellar emission model

2.1 Direct likelihood approach

This approach is conceptually similar to what was done before [4], but does not use the HI or CO templates at all (so it does not use the ring structure for the Milky Way). On the other hand, it adds more freedom to the data-based part. The gas structure is based on the dust map from Planck [5]. Even though the dust is not directly proportional to the gas column density that is needed for γ-ray emission, it has the big advantage of seeing all the gas (contrary to HI and CO), at a sufficient angular precision (1/8°). The radial dependence of the dust-to-gas ratio (increasing inwards) is actually comparable to that of the CR intensity, so the two effects compensate.

Figure 1 illustrates the approach that is taken. Since a significant fraction of sources near the Galactic plane are soft and unassociated (SGU in [1]) and could be due to mismodeled diffuse emission, we do not include them in the source component. Starting from π_0-decay and inverse Compton (IC) spectra, we adjust the residual maps to fit the sky, then fix those maps and adjust the spectra (this allows fitting bremsstrahlung emission), and proceed iteratively. This assumption of uniform spectrum for each template is not good enough for the dominant gas component, so we add spectral freedom, in the form of spatially dependent low-energy and high-energy power-law modulations. The maps of those parameters γ_1 and γ_2 are smoothed to avoid fluctuations. Hard features like the Fermi bubbles are fit via these modulations.

2.2 Approach using Information Field Theory (IFT)

Preliminary modeling of the diffuse emission within the IFT framework is carried out as follows. We use the instrument response function and exposure to prepare counts maps of diffuse and source (point-like and extended) components. We ingest the sources from the 4FGL catalog, templates for emission from the sun and the moon, held fixed for now. For diffuse emission, we use interstellar emission maps prepared with GALPROP [6] estimating emission from π_0-decay, IC, and bremsstrahlung components. These GALPROP components are tabulated in Galactocentric

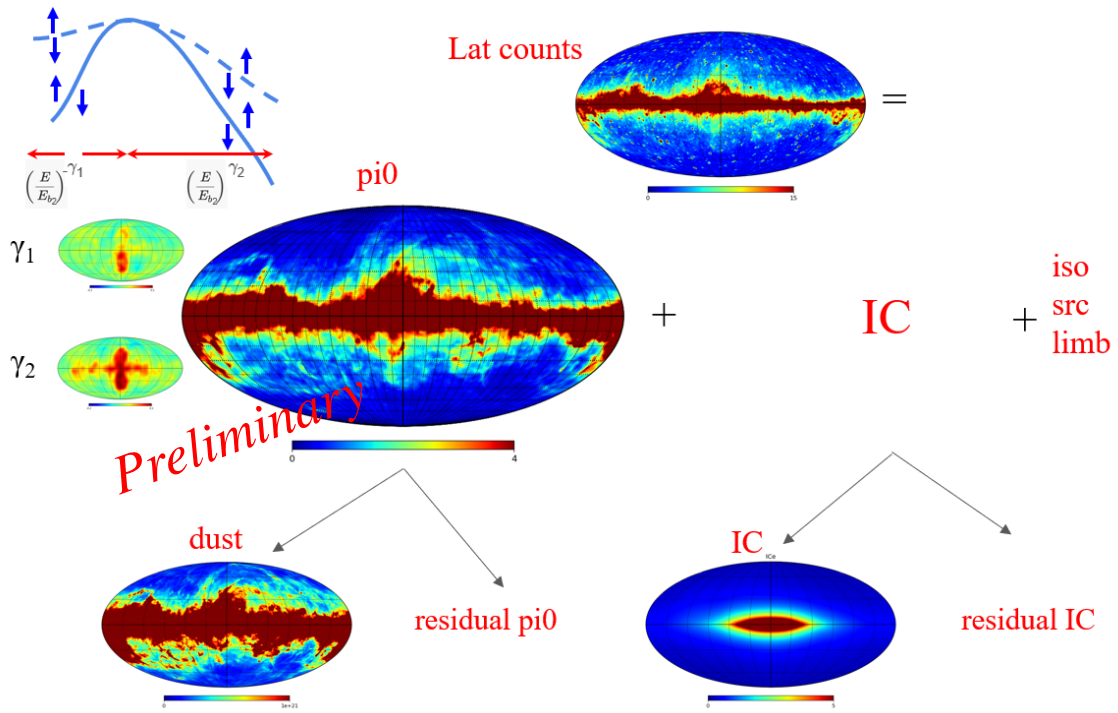

Figure 1: Sky decomposition adopted in the direct likelihood approach. Beside the isotropic, the Earth limb and the sources, the LAT sky is decomposed into two spectral templates. The first one (left) is π_0-decay like, modulated by a low-energy power law (top small map) and a high-energy power law (bottom small map). It is the sum of π_0 emission from gas traced by the dust (below left), which contains the small interstellar structures, and a data-based residual. The second one (right) is softer and IC-like. It is the sum of the expected IC emission from CR electrons (below left) and a data-based residual. The color scales are saturated to emphasize faint features.

rings, but in the analyses reported here the rings are combined into single templates for the sky. We supplement them with a dark gas component as in the 4FGL diffuse model.

We carry out the modeling using NIFTy v8 [7, 8], which aims to make inferences about the underlying, idealized fields, as they manifest in finite-resolution, noisy measurements. We model fields representing the multiplicative deviation of the input templates from their true values. For each template, these fields are realized as the three parameters of a LogParabola spectrum and they are constrained to follow a power-law spatial distribution $P(k) \propto k^{-3}$, where k is the wavenumber corresponding to a mode of the fluctuation field. These diffuse components are then co-added to form a full model which is compared with the data via Poisson likelihood. The amplitudes of the fluctuations for each component are constrained by priors that are chosen to allow adequate description of the data without substantial overfitting. In some models, we include an isotropic component with a spectrum constrained to follow a power law, and a component which has no input spatial information but which is constrained to follow a hard spectrum. The resulting fields at an energy (2.37 GeV) at the center of the LAT energy range are illustrated in Figure 2.

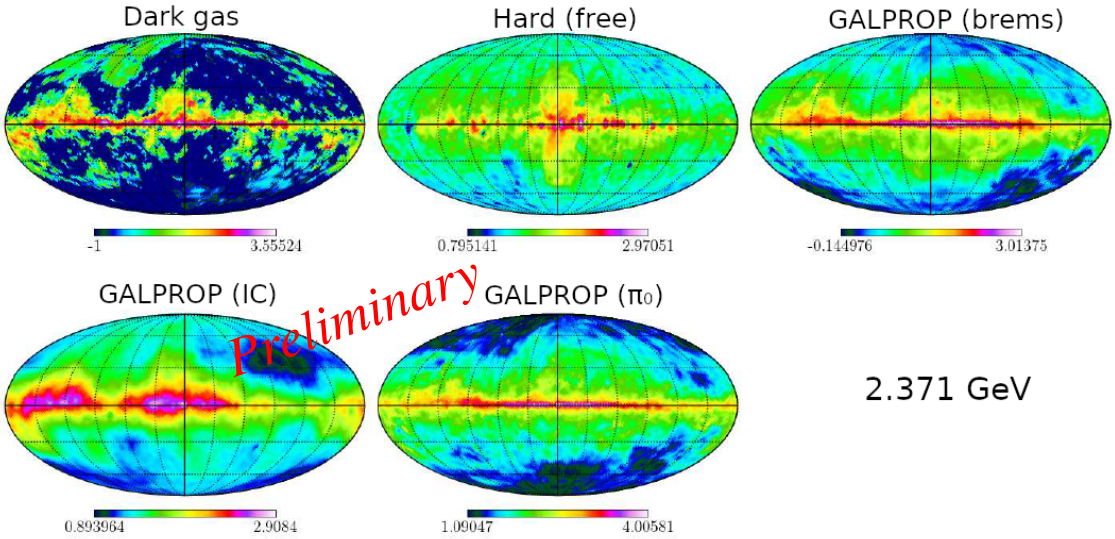

Figure 2: Sky decomposition adopted in the IFT approach. Five components are entered. The gas templates come from GALPROP (π_0, bremsstrahlung and IC separately). They are complemented by a dark gas template, and a free template to model hard residual features such as the Fermi bubbles. The color scales are in log(cts/pixel).

3. Preliminary source list

3.1 List of seeds, thresholding and light curves

The list of seeds was built using *pointlike*, as in previous catalogs. We did not update the list of extended sources, except that we used the two-template model of the Cygnus Loop [9] to reduce residuals there. We updated the list of transients to add 4 new faint transients from the last two years (three flares and nova V1723 Sco 2024). The all-sky verification led to adding nine point sources inside extended sources to account for strong residuals (in particular one in W 51C), and three fainter isolated peaks. Comparisons with DR4 associate sources using the 95% error ellipses and a minimum tolerance of 0.1°.

Figure 3 (left) shows that localization of faint sources at high latitudes (a relatively uniform sample) improves between 4FGL and FL16Y. This is not due to the additional exposure (because it compares comparably faint sources in both cases) but to the fact that going deeper moves the best sensitivity window to higher energy (trade-off between more background and more photons), where the angular resolution is better. Figure 3 (right) shows how the localization of individual sources improved (here mostly due to the additional exposure). A factor of 1.24 means a reduction by 1/3 of the area of the error ellipse. The large scatter in the distribution is due to source variability (some sources just got fainter in recent years) and additional confusion (there are 52% more sources in FL16Y than DR1).

We looked individually at all DR4 sources reported with bad spectral fit quality (i.e., disagreement between the global spectral fit and the SED points). A number of them were bright sources whose spectral representation could be improved, avoiding low-energy residuals that could affect neighbors. They came in two categories:

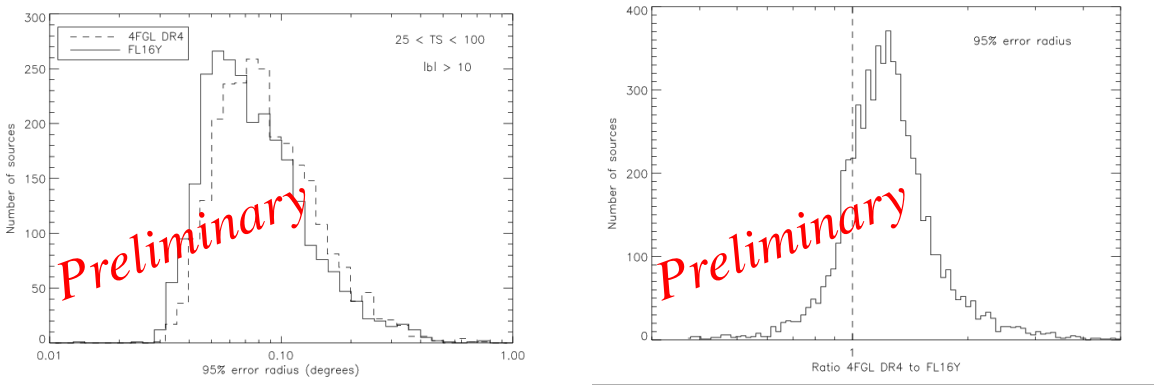

Figure 3: Localization improvement between 4FGL and FL16Y. Left: Error radius distribution in FL16Y (solid) compared to 4FGL-DR4 (dashed), restricted to sources at low TS and high-latitude (comparable). The means are 4.6' and 5.3', respectively. Right: Distribution of the ratio of error radii for the same sources in DR4 and FL16Y. The mean is 1.24.

1. Three sources could not be represented well by a single component: the γ-ray binaries LS I +61 303 and LS 5039, and the core of the Cen A radio galaxy. We added a hard power-law spectral component to all three. Sources split into two components appear in the catalog twice, with suffixes A and B, in order of decreasing significance. We also switched the two binaries to PLEC4 with free exponential index, because they drop fast toward high energies, but look like power laws at low energies.

2. Five other sources dropped fast toward high energies, but looked like power laws at low energies: four distant blazars affected by EBL absorption, and the black-widow pulsar candidate 1FGL J0334.2+7501. We switched them from LogParabola to PLEC4 with exponential index fixed to 1.

We also freed the exponential index in 6 more pulsars, and switched two bright blazars (Ton 599 and BL Lac) from LogParabola to PLEC4 with free exponential index.

Among the nearly 11,800 input point-source seeds, we kept 7,130 that reached TS > 25 in the *gtlike* pipeline, as before. This is about 5% more than point sources at TS > 25 in DR4. More than 6400 DR4 point sources (90%) are in FL16Y, including more than 110 at TS < 25 in DR4. Only the transients were allowed to remain at TS < 25 in FL16Y.

Light curves were generated as in DR4, with yearly time bins. 1992 sources are formally variable (probability less than 1% of being constant). This corresponds to 28% of the point sources, vs a little more than 26% in DR4. Most are blazars, as before.

3.2 Spectral energy distributions

The generation of Spectral Energy Distributions (SED) is the only part of the analysis that changed significantly since the DR4 catalog. The previous one suffered from serious limitations at low energy (in the first two bands mostly, below 300 MeV). The problems at low energy are due to the very broad PSF (68% containment radius of 2.2° at 300 MeV, 8.7° at 50 MeV). It leads to a low source-to-background ratio and a large confusion (the average distance between sources

is less than 1.5°). It also makes iterations in those bands very slow and unstable, and sometimes results in failures due to convergence errors. The previous method assumed nothing on the source fluxes (ie, each band was treated independently). This ensured absolute independence between the SED points. But it meant that nothing prevented a faint source with a relatively hard spectrum to become formally bright at low energy (with very large error bars). This is of course not prevented by any physical law (very soft sources with a high energy tail can exist) but attributing that flux to a brighter softer source just next would be a simpler physical solution. The idea of the new approach is to use information from the global spectral fit (over all energies) to set (Gaussian) priors when fitting the SED points, penalizing large excursions away from the global model.

Defining a prior mean is easy; it will just be the model prediction. Defining a prior sigma, however, requires careful attention in order not to overconstrain the SED fits, rendering the SED points useless as a check of the global spectral fit. To that end, the prior sigma σ_P is obtained as a combination of four terms, so that the largest one applies.

$$\sigma_P = \sqrt{\alpha^2\sigma_C^2 + \alpha^2\sigma_S^2 + \sigma_M^2 F_M^2 + F_M^2} \tag{1}$$

The first term σ_C is the covariance error, directly obtained from propagating the covariance matrix on the parameters of the global spectral model. The second term σ_S is the statistical error, what one would get from Poisson statistics (including likelihood weights) if the source was alone on a flat background. It is normally smaller than σ_C at low energy, but acts as a security when the model prediction is very low (very curved model fit). The first two terms are multiplied by a coefficient α, currently set to 3, so that the prior is first felt at about 3σ. The third term σ_M is the model error. It applies only to the power-law fits, which have only one spectral parameter and therefore smaller covariance errors than the LogParabola fits. It is obtained in relative terms as $\sigma_M = \ln(F_{LP}/F_M)$, where F_{LP} is the model prediction of the best LogParabola fit and F_M is the main (power-law) model fit. Finally, the fourth term is just the model prediction, so that the relative error on the final SED point if the data is not constraining at all is at least one. We do not apply the priors above 10 GeV, in a range where the PSF is good enough that the background is low and the confusion small.

Figure 4 compares the prior σ_P obtained from Eq.1 with the error obtained without priors in DR4 (that check was done in preparation shortly after DR4). It shows that, as required, the prior will have a strong effect in band 1, less strong in band 2, and not much effect in higher-energy bands, where confusion is much less. It also shows that the largest effect in band 1 is obtained for the hardest sources. Figure 5 illustrates the effect on one particular source. Figure 6 illustrates the error reduction on all sources in the first band.

Acknowledgments

The *Fermi*-LAT Collaboration acknowledges support for LAT development, operation and data analysis from NASA and DOE (United States), CEA/Irfu and IN2P3/CNRS (France), ASI and INFN (Italy), MEXT, KEK, and JAXA (Japan), and the K.A. Wallenberg Foundation, the Swedish Research Council and the National Space Board (Sweden). Science analysis support in the operations phase from INAF (Italy) and CNES (France) is also gratefully acknowledged. This work performed in part under DOE Contract DE-AC02-76SF00515.

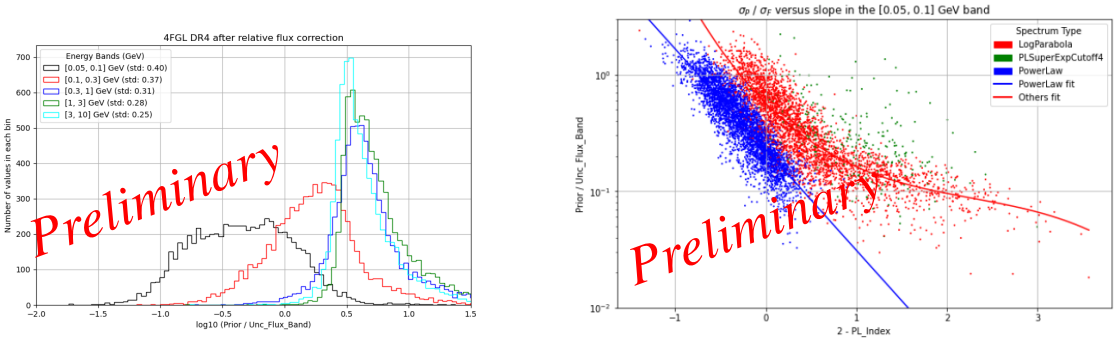

Figure 4: Prior σ_P to band fluxes compared to the errrors in the SED calculation without priors, on DR4 sources. Left: Distributions of the ratio between σ_P and SED error in all bands. The average ratio increases from band 1 to band 4 (best constraints), and decreases again in higher-energy bands. It is less than one (so the prior has a strong impact) in many sources in bands 1 and 2 only. The numbers in parentheses are the widths (standard deviation) of the distributions. Right: Correlation between that ratio and the spectral index in band 1 only, separately for each spectral type used in the model. For LogParabola, 2−PL_Index is replaced by the average index in νF_ν between band 1 and the pivot frequency ν_0, i.e. $1 + \ln(F_\nu(\nu_1)/F_\nu(\nu_0))/\ln(\nu_1/\nu_0)$, where ν_1 is the band center (in log). The ratio decreases from soft to hard sources in the first band, because hard sources are constrained by higher energies.

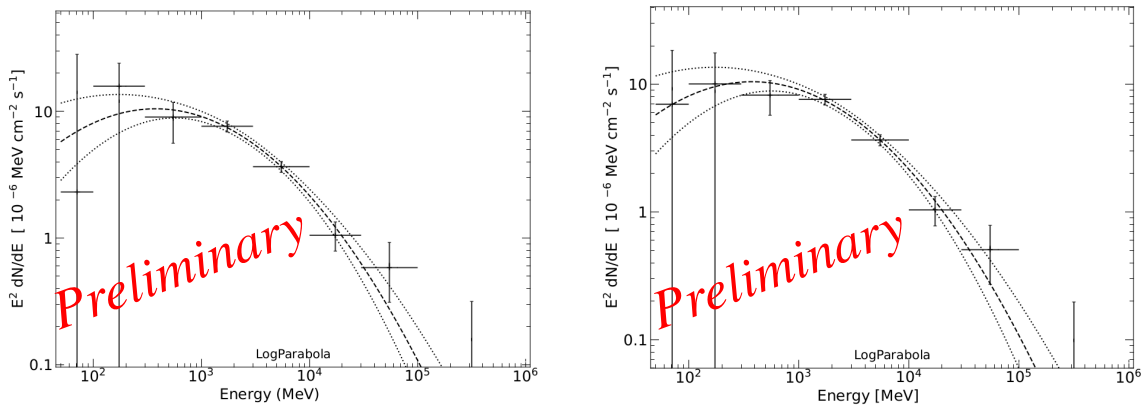

Figure 5: SED of 4FGL J1641.0−4619 (HESS J1641−463) in the official DR4 catalog (left) and after applying priors (right). The effect of the priors is obvious in the first two bands. The very uncertain SED points in DR4 have been pulled very close to the model prediction (dashed curve) and the errors have been somewhat reduced. The effect in the other bands (above 300 MeV) is small.

References

[1] S. Abdollahi, F. Acero, L. Baldini, J. Ballet, D. Bastieri et al., *Incremental Fermi Large Area Telescope Fourth Source Catalog*, ApJS **260** (2022) 53 [2201.11184].

[2] J. Ballet, P. Bruel, T.H. Burnett, B. Lott and The Fermi-LAT collaboration, *Fermi Large Area Telescope Fourth Source Catalog Data Release 4 (4FGL-DR4)*, *arXiv e-prints* (2023) arXiv:2307.12546 [2307.12546].

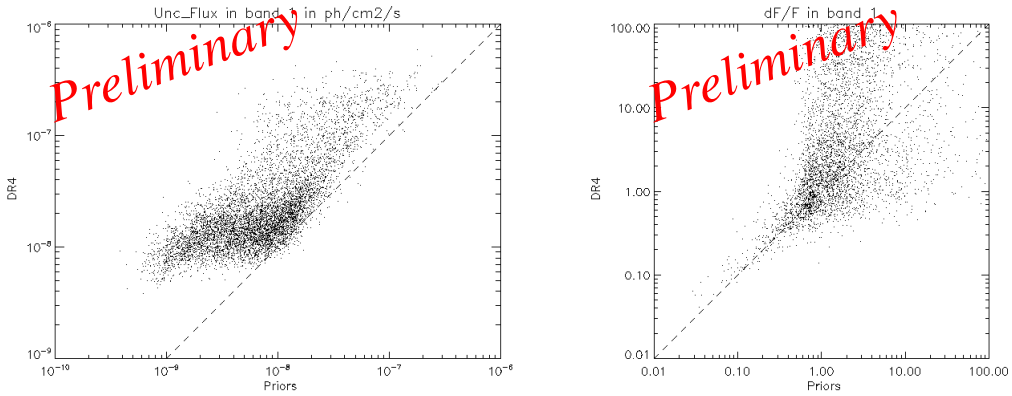

Figure 6: Effect of the priors on the errors in band 1 (50 to 100 MeV). It is illustrated on the upper errors, because the lower errors are truncated when the best fit is close to 0. Left: Direct correlation between the errors with priors (abscissa) and the original errors (ordinate). The dashed line is the one-to-one correlation. Essentially all points are above the line, indicating that the errors are reduced. The maximal reduction is approximately a factor ten. Right: Correlation of the relative errors (with respect to the best fit). The plot looks very different because the best fit changes as well. The effect, as expected, is largest for faint sources ($dF/F > 1$), and becomes smaller for strong ones. The very strong sources ($dF/F < 0.1$) tend to be all above the one-to-one correlation, corresponding to smaller errors with priors. This is not a direct effect of the priors (the prior sigma is always at least as large as the flux itself). It is instead an indirect consequence of forbidding fainter nearby sources to rise too much above their global models, as intended.

[3] S. Abdollahi, F. Acero, M. Ackermann, M. Ajello, W.B. Atwood et al., *Fermi Large Area Telescope Fourth Source Catalog*, ApJS **247** (2020) 33 [1902.10045].

[4] F. Acero, M. Ackermann, M. Ajello et al., *Development of the Model of Galactic Interstellar Emission for Standard Point-source Analysis of Fermi Large Area Telescope Data*, ApJS **223** (2016) 26 [1602.07246].

[5] Planck Collaboration, N. Aghanim, M. Ashdown et al., *Planck intermediate results. XLVIII. Disentangling Galactic dust emission and cosmic infrared background anisotropies*, A&A **596** (2016) A109 [1605.09387].

[6] T.A. Porter, G. Jóhannesson and I.V. Moskalenko, *The GALPROP Cosmic-ray Propagation and Nonthermal Emissions Framework: Release v57*, ApJS **262** (2022) 30 [2112.12745].

[7] M. Selig, M.R. Bell, H. Junklewitz, N. Oppermann, M. Reinecke, M. Greiner et al., *NIFTY - Numerical Information Field Theory. A versatile PYTHON library for signal inference*, A&A **554** (2013) A26 [1301.4499].

[8] L.I. Scheel-Platz, J. Knollmüller, P. Arras, P. Frank, M. Reinecke, D. Jüstel et al., *Multicomponent imaging of the Fermi gamma-ray sky in the spatio-spectral domain*, A&A **680** (2023) A2 [2204.09360].

[9] A. Tutone, J. Ballet, F. Acero, A. D'Aì and G. Cusumano, *Multiple accelerated particle populations in the Cygnus Loop with Fermi-LAT*, A&A **656** (2021) A139 [2109.15238].